INTERNATIONAL JOURNAL OF
NUMERICAL ANALYSIS AND MODELING
Volume 10, Number 2, Pages 298–313

THE IMMERSED FINITE ELEMENT METHOD FOR PARABOLIC PROBLEMS USING THE LAPLACE TRANSFORMATION IN TIME DISCRETIZATION

TAO LIN AND DONGWOO SHEEN

Abstract. In this paper we are interested in solving parabolic problems with a piecewise constant diffusion coefficient on structured Cartesian meshes. The aim of this paper is to investigate the applicability and convergence behavior of combining two non-conventional but innovative methods: the Laplace transformation method in the discretization of the time variable and the immerse finite element method (IFEM) in the discretization of the space variable. The Laplace transformation in time leads to a set of Helmholtz-like problems independent of each other, which can be solved in highly parallel. The employment of immerse finite elements (IFEs) makes it possible to use a structured mesh, such as a simple Cartesian mesh, for the discretization of the space variable even if the material interface (across which the diffusion coefficient is discontinuous) is non-trivial. Numerical examples presented indicate that the combination of these two methods can perform optimally from the point of view of the degrees of polynomial spaces employed in the IFE spaces.

Key words. Immersed finite element method, interface problems, Laplace transform, parallel algorithm

1. Introduction

We consider solving the following parabolic interface problem:

$$\frac{\partial u}{\partial t} - \nabla \cdot a(\mathbf{x})\nabla u = f(\mathbf{x},t), \quad (\mathbf{x},t) \in \Omega \times (0,T), \tag{1.1a}$$

$$u(\mathbf{x},t) = g(\mathbf{x},t), \quad (\mathbf{x},t) \in \partial\Omega \times (0,T), \tag{1.1b}$$

$$u(\mathbf{x},0) = u_0(\mathbf{x}), \quad \mathbf{x} \in \Omega, \tag{1.1c}$$

where the domain Ω is decomposed into two subdomains Ω^+ and Ω^- by an interface γ such that $\overline{\Omega} = \overline{\Omega^+} \cup \overline{\Omega^-}$ with $\Omega^+ \cap \Omega^- = \emptyset$. In (1.1), the diffusion coefficient $a(\mathbf{x})$ is a piecewise constant function such that

$$a(\mathbf{x}) = \begin{cases} a^- > 0, & \mathbf{x} \in \Omega^-, \\ a^+ > 0, & \mathbf{x} \in \Omega^+, \end{cases}$$

with $a^- \neq a^+$ in general; see Figure 1 for an illustration.

The discontinuity in the coefficient $a(\mathbf{x})$ leads to the following interface jump conditions to be satisfied by $u(\mathbf{x},t)$:

$$[u]_\gamma = 0 \quad \text{and} \quad \left[a\frac{\partial u}{\partial \mathbf{n}}\right]_\gamma = 0, \tag{1.2}$$

where $\mathbf{n}$ is the unit normal on the interface γ towards Ω^+.

In this paper, we apply two non-conventional but innovative approaches in solving (1.1). The time discretization is accomplished by the Laplace transformation method and the space discretization is carried out through the immersed finite

Received by the editors April 8, 2010 and, in revised form, January 4, 2012.
2000 *Mathematics Subject Classification.* 65N30, 44A10, 35K20.
This research work is partially supported by NSF grant DMS-0713763, DMS-1016313, NRF-2008-C00043 and NRF-2009-0080533.

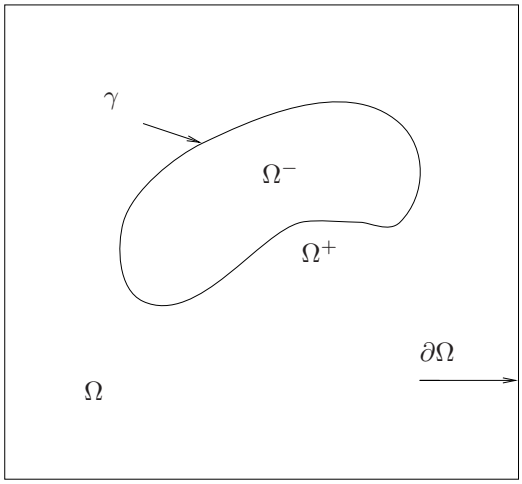

FIGURE 1. The domain Ω of the interface problem is separated by the interface γ across which the coefficient has a jump discontinuity.

element methods (IFEMs). The Laplace transformation approach allows us to generate an approximate solution to the parabolic initial boundary value problem (IBVP) through the solutions to a set of independent Helmholtz-like interface problems. In addition, IFEMs allow us to use interface independent meshes, such as structured Cartesian meshes if preferred, to solve parabolic IBVPs whose diffusion coefficients are discontinuous.

Instead of solving the parabolic problem (1.1) by using traditional time-marching algorithms, such as the backward Euler scheme and the Crank-Nicolson scheme, we apply the Laplace transformation method for the discretization in the time direction. For each z on a suitable contour $\Gamma \subset \mathbb{C}$, we denote by $\widehat{u}(\mathbf{x}, z)$ the standard Laplace transform in time of a function $u(\mathbf{x}, t)$:

$$\widehat{u}(\cdot, z) := \mathcal{L}[u](z) = \int_0^\infty u(\cdot, t) e^{-zt}\, dt. \tag{1.3}$$

The Laplace transforms of (1.1) are then given in the form

$$\begin{aligned} z\widehat{u}(\mathbf{x}, z) - \nabla \cdot\, a(\mathbf{x}) \nabla\, \widehat{u}(\mathbf{x}, z) &= u_0(\mathbf{x}) + \widehat{f}(\mathbf{x}, z), \\ &\qquad (\mathbf{x}, z) \in \Omega \times \Gamma, \qquad (1.4a) \\ \widehat{u}(\mathbf{x}, z) &= \widehat{g}(\mathbf{x}, z), \\ &\qquad (\mathbf{x}, z) \in \partial\Omega \times \Gamma. \qquad (1.4b) \end{aligned}$$

For each $z \in \Gamma$, let $\mathcal{S}(z) : L^2(\Omega) \times H^{1/2}(\partial\Omega) \to H^1(\Omega)$ be the solution operator associated with the above complex-valued Helmholtz-like problem (1.4) so that

$$\widehat{u}(\cdot, z) = \mathcal{S}(z) \left(u_0(\cdot) + \widehat{f}(\cdot, z), \widehat{g}(\cdot, z) \right). \tag{1.5}$$

By the *Laplace inversion formula* ([3]), the time-domain solution to the parabolic interface problem (1.1) is given by

$$\begin{aligned} u(\cdot, t) &= \frac{1}{2\pi \mathrm{i}} \int_\Gamma \widehat{u}(\cdot, z) e^{zt}\, dz \qquad (1.6a) \\ &= \frac{1}{2\pi \mathrm{i}} \int_\Gamma \mathcal{S}(z) \left(u_0(\cdot) + \widehat{f}(\cdot, z), \widehat{g}(\cdot, z) \right) e^{zt}\, dz. \qquad (1.6b) \end{aligned}$$

It should be stressed that the procedure of solving (1.4) for a number of z's on Γ is easily parallelizable since in calculating (1.5) for a z is completely independent of calculating it for other z's.

Moreover, by choosing a suitably deformed contour Γ, one can stabilize the Laplace inversion (1.6) which can also enhance convergence significantly. Such an idea of using the Laplace transformation to solve parabolic problems has been developed actively after [26, 27], which emphasized the nature of parallelization as well as the deformation of the contour Γ to improve stability and convergence. This thread of thoughts has been analyzed and improved in [10, 16, 17, 25, 29, 31] and the references therein. Since the Laplace transformation method is highly accurate in time discretization, it is natural to keep a balance between time and space discretizations. An investigation in this direction has been carried out in [7], where some high-order compact finite difference schemes are used for space discretization and the Laplace transformation method is adopted in time discretization; the resulting linear systems are solved using Madpack (a multigrid solver [6]) and QMR (quasi-minimal residual methods [9]).

In solving the interface problems (1.4) by the finite element method, one needs to take a special care around the interface γ in order to balance the spatial discretization errors generated near the interface and those generated far from the interface. Typical remedies are to employ locally fitted finite elements and adaptive finite elements. Although these methods are very effective, one drawback is that the meshes are seriously distorted, and thus the mesh generation requires some additional nontrivial labors. Another approach, instead, is to adopt the IFEM based on Cartesian meshes independent of the interface. The idea of IFEM is to fit the jump conditions described in (1.2) inside each element by modifying the standard finite element basis ϕ such that

$$[\phi]_\gamma = 0 \quad \text{and} \quad \left[a\frac{\partial \phi}{\partial \mathbf{n}}\right]_\gamma = 0.$$

Since the 1D linear IFEM [18] was announced, the 2D linear IFEM [19, 20, 28], the 3D linear IFEM [14], the bilinear IFEM [21], a quadratic IFEM [4] and an arbitrarily higher-order 1D IFEM [2] have been developed. Convergence analysis has been carried out in [2, 12, 19, 22]. The idea of IFE spaces has been applied to Galerkin methods, finite volume methods, and discontinuous Galerkin methods [1, 2, 4, 8, 11, 13, 14, 18, 20, 21] to solve elliptic interface problems. For the application of the IFEMs to some engineering problems, readers are referred to [15, 23, 24, 30].

The organization of the paper is as follows. In the section to follow the Laplace transformation method is applied to the discretization in time variable. In §3 the IFEM is applied to solve the resulting complex-valued elliptic interface problems. Numerical results are shown in §4 to illustrate feature of this new approach for solving parabolic problems with discontinuous coefficients. Conclusions are drawn in the last section.

2. The Laplace transformation method

In this section we briefly review the Laplace transformation method for solving parabolic problems and how it can be used to carry out the discretization in time.

The idea of finding an exact solution for (1.1) by solving the Laplace transformed equations (1.4) goes back to Thomas John I'Anson Bromwich [3] in 1917. Although Bromwich did not define or mention the notion of Laplace transformation (1.3)

explicitly, what he used was exactly the identical framework of inverse Laplace transformation, as given in (1.6a). It was Gustav Deutsch who started to call (1.3) as "Laplace transform" and studied intensively in his well-known monograph [5] published in 1937. Noticeably Bromwich proved that the Laplace inversion (1.6a) using a straight line contour parallel to the imaginary axis,

$$\Gamma = \{z \in \mathbb{C} : z(\omega) = \zeta_c + \mathrm{i}\omega, \text{ where } \omega \in \mathbb{R} \text{ increases from } -\infty \text{ to } +\infty\}, \tag{2.1}$$

was equal to that using any deformed contour as long as all the singularities of the integrand, whose real parts are less than ζ_c, lie to the left of the new contour, still denote by Γ. We represent the deformed contour Γ using the following parameterization:

$$\Gamma = \{z \in \mathbb{C} : z(\omega) = \zeta(\omega) + \mathrm{i}s\omega, \quad \omega \in \mathbb{R}\}, \tag{2.2}$$

where $\zeta : \mathbb{R} \to \mathbb{R}$ is an increasing, continuous function and s is a parameter. For such examples, see the graphs on the left and right in Figure 2, respectively.

2.1. Deformation of the contour. Although the two contour integrals obtained by using a straight line contour of type (2.1) and a deformed contour of type (2.2) are identical, their numerical approximation errors can be significantly different. In evaluating the integral in (1.6) numerically, the integrand, containing the exponential part e^{zt}, will suffer from an oscillatory behavior, as the imaginary part of z along the contour Γ goes to $\pm\infty$. This is one of the main sources of numerical instability, which can be more tamed if the real part of z becomes smaller. This feature will be culminated if the real part of z gets negative. Based on this, Sheen *et al.* [27] proposed a hyperbola contour by choosing $\zeta(\omega) = \alpha - \sqrt{\omega^2 + \beta^2}$ in (2.2). In this case, since the contour cuts the real line at $\alpha - \beta$, α and β must be selected such that $\alpha - \beta$ is larger than the negative of the smallest eigenvalue of the elliptic operator $A \equiv -\nabla \cdot a(\mathbf{x})\nabla$ and the real parts of singularities of $u_0 + \widehat{f}(z)$. Also s should be chosen such that all the singularities of $\widehat{u}(\cdot, z)$ are to the left of the contour Γ. Using such a hyperbola contour, the inversion formula (1.6) becomes an infinite integral with respect to the real variable ω as follows:

$$\begin{aligned} u(\cdot,t) &= \frac{1}{2\pi\mathrm{i}} \int_{-\infty}^{\infty} \widehat{u}(\cdot, z(\omega)) e^{z(\omega)t} z'(\omega) \mathrm{d}\omega \\ &= \frac{1}{2\pi\mathrm{i}} \int_{-\infty}^{\infty} \widehat{u}(\cdot, \zeta(\omega) + \mathrm{i}s\omega) e^{(\zeta(\omega)+\mathrm{i}s\omega)t} (\zeta'(\omega) + \mathrm{i}s) \mathrm{d}\omega. \end{aligned} \tag{2.3}$$

The next step is to transform the infinite domain, $(-\infty, \infty)$, of the above integration (2.3) into any convenient finite interval, *e.g.*, $[-1, 1]$, on which a numerical quadrature will be applied. There are of course infinitely many possible transformations to accomplish this, each of which determines a different distribution of graded quadrature points on the contour Γ. To be specific, we use the change of variables $y = \psi(\omega) = \tanh(\frac{\tau\omega}{2})$ mapping from $(-\infty, \infty)$ to $[-1, 1]$, with its inverse given by

$$\omega(y) = \psi^{-1}(y) = \frac{2}{\tau} \tanh^{-1}(y) = \frac{1}{\tau} \log \frac{1+y}{1-y}, \tag{2.4}$$

where $\tau > 0$ determines the gradedness of quadrature points such that the larger τ is chosen, the more points are concentrated near the real axis. The above change

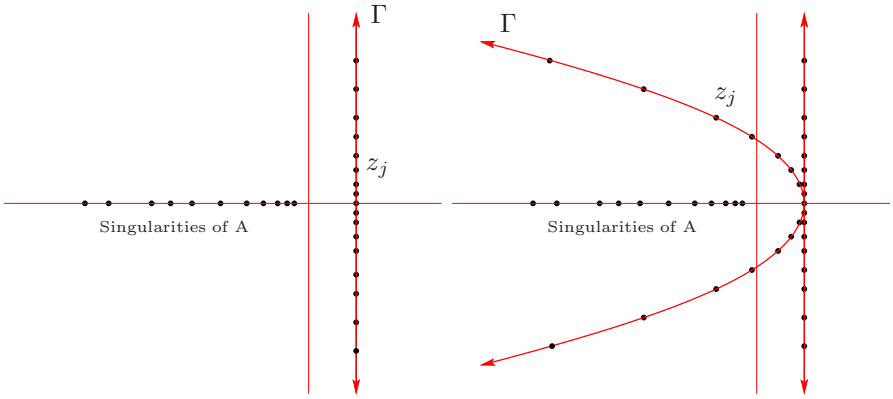

FIGURE 2. The contours used for the Laplace inversion.

of variables reduces the integral on an infinite interval in (2.3) to an integral on a finite interval as follows:

$$
\begin{aligned}
u(\cdot,t) &= \frac{1}{2\pi \mathrm{i}} \int_{-1}^{1} \widehat{u}(\cdot, z(\omega(y))) e^{z(\omega(y))t} z'(\omega(y))\omega'(y)\mathrm{d}y \\
&= \frac{1}{2\pi \mathrm{i}} \int_{-1}^{1} \widehat{u}(\cdot, \zeta(\omega(y)) + \mathrm{i}s\omega(y)) \\
&\qquad\qquad e^{(\zeta(\omega(y))+\mathrm{i}s\omega(y))t}(\zeta'(\omega(y)) + \mathrm{i}s)\omega'(y)\mathrm{d}y.
\end{aligned} \tag{2.5}
$$

Since $f(\mathbf{x},t)$ and $g(\mathbf{x},t)$ are real-valued functions, the solution $\widehat{u}(\mathbf{x},z)$ of (1.4) satisfies the conjugate relation:

$$
\overline{\widehat{u}(\mathbf{x},z)} = \widehat{u}(\mathbf{x},\overline{z}). \tag{2.6}
$$

Let Γ^+ and Γ^- denote the upper and lower half pieces of the contour Γ. Owing to (2.6) and the symmetry of the contour Γ with respect the real axis, the integral in (1.6) can be evaluated on Γ^+ as follows:

$$
\begin{aligned}
u(\cdot,t) &= \frac{1}{2\pi \mathrm{i}} \int_{\Gamma^+} \widehat{u}(\cdot,z) e^{zt}\, dz + \frac{1}{2\pi \mathrm{i}} \int_{\Gamma^-} \widehat{u}(\cdot,z) e^{zt}\, dz \\
&= \frac{1}{2\pi \mathrm{i}} \int_{\Gamma^+} \widehat{u}(\cdot,z) e^{zt}\, dz - \overline{\frac{1}{2\pi \mathrm{i}} \left(\int_{\Gamma^+} \widehat{u}(\cdot,z) e^{zt}\, dz \right)} \\
&= \frac{1}{\pi} \operatorname{Im} \left(\int_{\Gamma^+} \widehat{u}(\cdot,z) e^{zt}\, dz \right).
\end{aligned} \tag{2.7}
$$

A similar argument applies to (2.3) and (2.5). Consequently we have

$$
u(\cdot,t) = \frac{1}{\pi} \operatorname{Im} \Big(\int_0^1 \widehat{u}(\cdot, z(\omega(y))) e^{z(\omega(y))t} z'(\omega(y))\omega'(y)\mathrm{d}y \Big). \tag{2.8}
$$

2.2. Semi-discrete approximation. The last integral formula (2.8) in the previous section can be discretized by using a quadrature rule. Since the integrand and its derivatives will vanish at the upper limit of the integral, the composite trapezoidal rule will perform very well due to the Euler-McLaurin type behavior. Hence, we have the semi-discrete approximation of $u(\cdot,t)$ given by

$$
u_{N_z,\tau}(\cdot,t) = \frac{1}{\pi} \operatorname{Im} \Big(\sum\nolimits_{j=0}^{N_z-1} q_j \widehat{u}(\cdot,z_j) \frac{\mathrm{d}z}{\mathrm{d}\omega}(\omega_j) \frac{\mathrm{d}\omega}{\mathrm{d}y}(y_j) e^{z_j t} \Big), \tag{2.9}
$$

where $q_0 = \frac{1}{2N_z}, q_j = \frac{1}{N_z},\ 1 \le j \le N_z - 1$, are the quadrature weights with the corresponding quadrature nodes:

$$y_j = \frac{j}{N_z} \quad \text{for } j = 0, 1, \cdots, N_z - 1, \tag{2.10}$$

and

$$z_j = z(\omega_j), \quad \omega_j = \omega(y_j),\ j = 0, 1, \cdots, N_z - 1. \tag{2.11}$$

It is proved in [27] that the quadrature scheme (2.9) is of arbitrary high-order spectral convergence rate if in particular the source term f has high-order regularity, stated as follows:

Theorem 2.1 ([27]). *Let $u(\mathbf{x}, t)$ be the solution of (1.1) and let $u_{N_z,\tau}(\mathbf{x}, t)$ be its approximation defined by (2.9). Assume that $\widehat{f}(\cdot, z)$ is analytic to the right of the contour Γ and continuous onto Γ, with $\widehat{f}^{(j)}(\cdot, z)$ bounded on Γ for $j \le r$ and r an integer ≥ 1, Then, for $t > r\tau$*

$$\|u_{N_z,\tau}(t) - u(t)\| \le \frac{C_{r,s}}{N_z^r}\Big(1 + t^r + \frac{1}{\tau^r}\Big)e^{\gamma t}\Big(1 + \log_+ \frac{1}{t - r\tau}\Big) \Big(\|u_0\| + \max_{k \le r} \sup_{z \in \Gamma} \|\widehat{f}^{(k)}(z)\|\Big). \tag{2.12}$$

The implication of the above theorem without the source term f is that the scheme is of order $O(\frac{1}{N_z^r})$ with an arbitrarily large $r > 0$ whenever τ and t are chosen such that $\frac{t}{\tau}$ is sufficiently large. In this case, the discretization errors in the time direction by using the Laplace transformation method are negligible compared to those caused from the spatial discretization part.

We should point out that the summands of (2.9), $\widehat{u}(\cdot, z_j)\frac{\mathrm{d}z}{\mathrm{d}\omega}(\omega_j)\frac{\mathrm{d}\omega}{\mathrm{d}y}(y_j),\ j = 0, \cdots, N_z$, are independent of t. Therefore, we only have to generate an approximate solution to $\widehat{u}(\cdot, z_j)$ once by solving the complex-valued elliptic problem (1.4) for a set of $z_j, j = 0, 1, \cdots, N_z$. Then, the solution $u(\mathbf{x}, t)$ to (1.1) for any t in an interval can be generated very quickly by (2.9) from the set of already-computed spatial solutions $\widehat{u}(\cdot, z_j), j = 0, 1, \cdots, N_z$; the only modification is to change the multiplication factor $e^{z_j t}$ for the needed time t.

Also, we note that the elliptic problem (1.4) for each z_j from the set of $z_j, j = 0, 1, \cdots, N_z$, is independent of the other elliptic problems for the remaining z_j's. Modern multiprocessor computers can take a great advantage of this feature because each processor can be assigned to solve one of these boundary value problems, and the computation of $\widehat{u}(\cdot, z_j),\ j = 0, 1, 2, \cdots, N_z$, can be carried out in parallel without any communication between each solution procedure.

3. The immersed finite element method

Even though we believe that most of the immersed finite elements in the literature for 2nd order elliptic interface problems can be applied to solving parabolic interface problems, we survey only two classes of them in this section to present our main ideas.

3.1. The 1D p-th degree IFE space. For the 1D parabolic interface problems, we plan to use the p-th degree IFE space [1, 2] which is developed originally for

solving the following interface problem:

$$\begin{aligned} -(a(x)u'(x))' &= f(x),\ x\in\Omega=(0,1), && (3.1a)\\ u(0) &= u_l,\ u(1)=u_r, && (3.1b)\\ [u]_\gamma &= 0,\ [au']_\gamma = 0, && (3.1c)\end{aligned}$$

where we assume that the coefficient $a(x)$ is a piecewise constant function with one interface.

$$a(x)=\begin{cases} a^->0, & x\in\Omega^-=(0,\gamma),\\ a^+>0, & x\in\Omega^+=(\gamma,1).\end{cases}$$

The idea can be easily extended to handle the case in which $a(x)$ has multiple interfaces. Consider a family of mesh $\{\Omega_h\}_{0<h<1}$:

$$\begin{aligned} &\Omega_h: 0=x_0<x_1<\cdots<x_M=1,\\ &h_j=x_j-x_{j-1},\ 1\le j\le M,\ h=\max_{1\le j\le M}h_j.\end{aligned}$$

Without loss of generality, we assume that there is only one interface element, say $K_{j_\gamma}=(x_{j_\gamma-1},x_{j_\gamma})$ in Ω_h such that $\gamma\in K_{j_\gamma}$, while all the other elements are interface-free. On an element $K_j=(x_{j-1},x_j),\ 1\le j\le M$, we introduce $p+1$ auxiliary nodes:

$$x_{j-1}=t_{j,0}<t_{j,1}<\cdots<t_{j,p}<t_{j,p}=x_j,$$

and let $L_{j,k}(x),\ 0\le k\le p$, be the p-th degree Lagrange cardinal polynomials defined by these nodes. On each non-interface element $K_j,\ j\ne j_\gamma$, we define the local IFE space by

$$S_h(K_j)=\mathrm{span}\{\phi_{j,k}(x),\ 0\le k\le p\},\ \phi_{j,k}(x)=L_{j,k}(x),\ 0\le k\le p.$$

On the interface element K_{j_γ}, we construct the $p+1$ IFE functions $\phi_{j_\gamma,k}(x),\ 0\le k\le p$ as follows:

$$\begin{aligned} \phi_{j_\gamma,k}(x) &= \begin{cases}\phi^-_{j_\gamma,k}(x)\in\Pi_p, & x\in K^-_{j_\gamma}=(x_{j_\gamma-1},\gamma),\\ \phi^+_{j_\gamma,k}(x)\in\Pi_p, & x\in K^+_{j_\gamma}=(\gamma,x_{j_\gamma}),\end{cases}\\ \phi_{j_\gamma,k}(t_{j_\gamma,l}) &= \delta_{jl},\ 0\le l\le p,\\ \left[\phi_{j_\gamma,k}\right]_\gamma &= 0,\ \left[a\phi^{(l)}_{j_\gamma,k}\right]_\gamma=0,\ 1\le l\le p,\end{aligned}$$

where Π_p denotes the set of polynomials of degree not greater than p. It has been shown [2] that these IFE functions can be uniquely constructed and they are linearly independent. Set

$$S_h(K_{j_\gamma})=\mathrm{span}\{\phi_{j_\gamma,k}(x),\ 0\le k\le p\}$$

to be the local IFE space on the interface element K_{j_γ}. Finally, we can form the 1D p-th degree IFE space on Ω as follows:

$$S_h(\Omega)=\{v\in H^1(\Omega)\ \mid\ v|_{K_j}\in S_h(K_j),\ \forall K_j\in\Omega_h\},$$

where $S_h(K_j)$ is the p-th degree local IFE space described above.

3.2. The 2D linear IFE space. The 2D IFE space to be used is developed in [20] for the following interface problem:

$$\begin{aligned} -\nabla \cdot (a(\mathbf{x})\nabla u(\mathbf{x})) &= f(\mathbf{x}),\ \mathbf{x} \in \Omega \subset \mathbb{R}^2, && \text{(3.2a)} \\ u(\mathbf{x}) &= g(\mathbf{x}),\ \mathbf{x} \in \partial\Omega, && \text{(3.2b)} \\ [u]_\gamma &= 0,\ \left[a\frac{\partial u}{\partial \mathbf{n}}\right]_\gamma = 0. && \text{(3.2c)} \end{aligned}$$

Let $(\Omega_h)_{0\le h\le 1}$ be a family of triangular meshes of the domain Ω formed with nodes $\mathcal{N}_h \in \overline{\Omega}$. Note that Ω_h consists of two types of elements: (1) interface elements cut through by the interface γ; (2) non-interface elements. First, on each element $K = \triangle A_1A_2A_3 \in \Omega_h$, let $\phi_j(\mathbf{x}),\ j = 1, 2, 3$, be the standard linear polynomials such that

$$\phi_j(A_k) = \delta_{ik},\ k = 1, 2, 3.$$

Denote by $\Pi_1(K')$ the space of linear polynomials on a set $K' \subset \mathbb{R}^2$. If $K \in \Omega_h$ is a non-interface element, let the local IFE function space be the usual standard piecewise linear space $S_h(K) = \Pi_1(K)$ such that

$$S_h(K) = \text{span}\{\phi_1, \phi_2, \phi_3\} \quad \text{with } \phi_j(A_k) = \delta_{jk}.$$

On each interface element $K = \triangle A_1A_2A_3$, we construct 3 linear IFE basis functions $\widetilde{\phi}_j(\mathbf{x}),\ j = 1, 2, 3$, as follows:

$$\begin{aligned} &\widetilde{\phi}_j = \begin{cases} \widetilde{\phi}_j^- \in \Pi_1(K^-), & \mathbf{x} \in K^-, \\ \widetilde{\phi}_j^+ \in \Pi_1(K^+), & \mathbf{x} \in K^+, \end{cases} \\ &\widetilde{\phi}_j(A_k) = \delta_{jk},\ k = 1, 2, 3, \\ &[\widetilde{\phi}_j]_{\overline{DE}} = 0,\ \left[a\frac{\partial \widetilde{\phi}_j}{\partial \mathbf{n}_{\overline{DE}}}\right]_{\overline{DE}} = 0, \end{aligned}$$

where D and E are the two points where the interface γ intersects with the edge of the interface element K as shown in Figure 3.

Again, it can be shown that these linear IFE basis functions can be uniquely constructed [19, 20] and we define the local IFE function space on an interface element $K \in \Omega_h$ by

$$S_h(K) = \text{span}\{\widetilde{\phi}_1, \widetilde{\phi}_2, \widetilde{\phi}_3\}.$$

Finally, the 2D linear IFE space can be described as follows:

$$S_h(\Omega) = \{v \mid v|_K \in S_h(K)\ \forall K \in \Omega_h,\ v \text{ is continuous at all } \mathbf{x} \in \mathcal{N}_h\}.$$

3.3. The IFEM for the Laplace transformed equations. The weak formulation of the Laplace transformed equations (1.4) is given as follows: for each $z \in \Gamma$, find $\widehat{u} = \widehat{u}(\cdot, z) \in H^1(\Omega)$ such that

$$\begin{aligned} z(\widehat{u}, v) + (a\nabla \widehat{u}, \nabla v) &= \left(u_0 + \widehat{f}(\cdot, z), v\right),\ v \in H_0^1(\Omega), && \text{(3.3a)} \\ \widehat{u}(\mathbf{x}, z) &= \widehat{g}(\mathbf{x}, z),\ \mathbf{x} \in \partial\Omega. && \text{(3.3b)} \end{aligned}$$

Let $(\Omega_h)_{0<h<1}$ be a family of meshes of Ω whose elements have diameters bounded by h. Associated with Ω_h, let $S_h(\Omega)$ be an IFE space such as one of those discussed

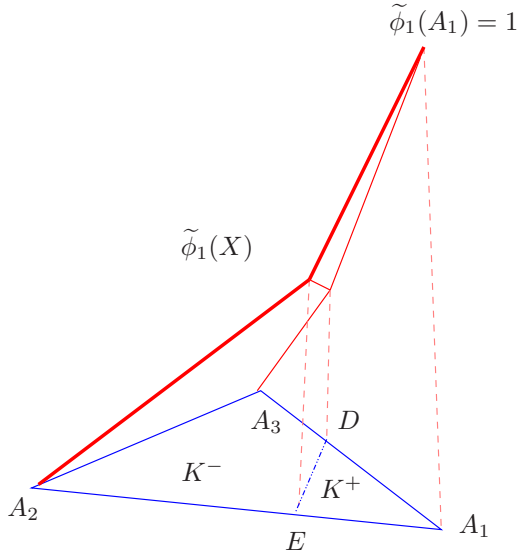

FIGURE 3. An interface basis function ϕ_1 on $\overline{K} = \overline{K^-} \cup \overline{K^+}$ whose gradient has a jump across the line $\overline{DE}$; $\widetilde{\phi}_1(A_j) = \delta_{1j}$.

in the previous subsections. The immersed finite element method for (3.3) is to find $\widehat{u}_h(\cdot, z) \in S_h(\Omega)$ such that for all $v_h \in S_{h,0}(\Omega)$, we have

$$\begin{aligned} z(\widehat{u}_h, v_h) + (a\nabla\,\widehat{u}_h, \nabla\, v_h) &= \left(u_0 + \widehat{f}(\cdot, z), v_h\right), \quad v_h \in S_{h,0}(\Omega), && \text{(3.4a)} \\ \widehat{u}_h(\mathbf{x}, z) &= \widehat{g}(\mathbf{x}, z), \ \forall \mathbf{x} \in \mathcal{N}_h \cap \partial\Omega, && \text{(3.4b)} \end{aligned}$$

with

$$S_{h,0}(\Omega) = \{v \mid v \in S_h(\Omega),\ v(\mathbf{x}) = 0\ \forall \mathbf{x} \in \mathcal{N}_h \cap \partial\Omega\}.$$

The IFE functions used here are designed for solving the elliptic interface problem (3.2); hence, they can perform well in discretization involving the term $(a\nabla\,\widehat{u}, \nabla\, v)$ in the weak form which contains the interface part. Furthermore, our numerical results confirm that these IFE functions are also suitable for the approximation in the mass matrix part resulted from the term $(\widehat{u}, v)$ as well.

4. Numerical Examples

In this section we present numerical examples to demonstrate features of our new method for solving the parabolic initial boundary problem (1.1) with a discontinuous coefficient in one and two dimensions.

We start with a summarization of our method:

Step 1: Choose suitable parameters $\alpha,\ \beta,\ s$ and τ to be used in (2.2) and (2.4).
Step 2: Choose the number of control points N_z, generate $y_j,\ 0 \le j \le N_z - 1$ by (2.10) and the corresponding $\omega_j,\ z_j,\ 0 \le j \le N_z - 1$ by (2.2) and (2.4), respectively.
Step 3: Choose a suitable mesh parameter h for the discretization in $\mathbf{x}$ variable and generate $\widehat{u}_h(\mathbf{x}, z_j),\ 0 \le j \le N_z - 1$ by (3.4).

Step 4: Generate $u_h(\mathbf{x},t) \approx u(\mathbf{x},t)$ by (2.9) with $\widehat{u}_h(\mathbf{x},z_j) \approx \widehat{u}(\mathbf{x},z_j)$, $0 \le j \le N_z - 1$.

4.1. A 2D numerical example. We consider the parabolic IBVP (1.1) posed on $\Omega = (-1,1)^2$ which is separated by the interface γ into two sub-domains $\Omega^- = \{\mathbf{x} : |\mathbf{x}| < r_0\}$ and $\Omega^+ = \Omega \backslash \overline{\Omega^-}$ with $r_0 = \pi/6.28$. The coefficient function $a(x,y)$ is chosen as a piecewise constant function

$$a(\mathbf{x}) = \begin{cases} a^- = 10, & \mathbf{x} \in \Omega^-, \\ a^+ = 1, & \mathbf{x} \in \Omega^+. \end{cases}$$

We define

$$w(\mathbf{x}) = \begin{cases} \frac{|\mathbf{x}|^3}{a^-}, & \mathbf{x} \in \Omega^-, \\ \frac{|\mathbf{x}|^3}{a^+} - \left(\frac{1}{a^-} - \frac{1}{a^+}\right) r_0^3, & \mathbf{x} \in \Omega^+. \end{cases} \tag{4.1}$$

By direct verification, we see that $w(\mathbf{x})$ satisfies the jump conditions across the interface γ:

$$[w]_\gamma = 0 \quad \text{and} \quad \left[a \frac{\partial w}{\partial \mathbf{n}}\right]_\gamma = 0.$$

Then, we set $u(\mathbf{x},t) = w(\mathbf{x}) e^{-\delta t}$ with $\delta = 0.1$ as the exact solution to the parabolic problem (1.1) from which we can generate the following data functions:

$$f(\mathbf{x},t) = \left[-\delta w(\mathbf{x}) - \nabla \cdot (a(\mathbf{x}) \nabla w(\mathbf{x}))\right] e^{-\delta t}, \quad g(\mathbf{x},t) = u(\mathbf{x},t),$$

and the initial condition given by $u_0(\mathbf{x},0) = w(\mathbf{x})$.

In the numerical results reported below, the following parameters are used:

$$\alpha = 1.25,\ \beta = 0.25,\ s = 0.45, \tau = 0.5.$$

Unless otherwise specified, $N_z = 40$ points are employed to approximate the contour integration in all the two dimensional numerical experiments. Also, in the linear IFEM used for solving the complex-valued elliptic interface problems we use uniform triangular meshes Ω_h formed by first partitioning Ω into squares with edge length h and further partitioning each square into two triangles along a diagonal line.

The errors in $u_h(\mathbf{x},t)$ measured by both L^2-norm and H^1-seminorm for time $t = 0.5, 1, 2, \cdots, 6$, are shown in Tables 1 and 2, respectively.

From these numerical experiments, we note that once the set of complex-valued IFE solutions $\widehat{u}_h(\mathbf{x},z_j), j = 0, 1, \cdots, N_z - 1$ for the elliptic interface problems are obtained by solving (3.4), the approximation $u_h(\mathbf{x},t)$ to $u(\mathbf{x},t)$ can be generated by the numerical inversion (2.9) with $\widehat{u}(\mathbf{x},z_j)$ replaced by $\widehat{u}_h(\mathbf{x},z_j)$ very quickly because $u_h(\mathbf{x},t)$ is simply a linear combination of $\widehat{u}_h(\mathbf{x},z_j), j = 0, 1, \cdots, N_z - 1$. Secondly, we notice that once this set of complex-valued IFE solutions $\widehat{u}_h(\mathbf{x},z_j), j = 0, 1, \cdots, N_z - 1$ are prepared, they can be used to generate the solution $u(\mathbf{x},t)$ for a rather large range of values of t.

For this example, the data in Table 1 indicate that the 40 IFE solutions $\widehat{u}_h(\mathbf{x},z_j)$, $j = 0, 1, \cdots, 39$, can produce approximation to $u(\mathbf{x},t)$ with the optimal $O(h^2)$-convergence rate in the L^2 norm for any $t \in [1,5]$. This scheme seems to become sub-optimal when t is outside of $[1,5]$ as suggested by the data at $t = 0.5$ and $t = 6$ in Table 1. On the other hand, as demonstrated by the data in Table 2, if we measure the error by the H^1-seminorm, these IFE solutions can produce optimal approximation to $u(\mathbf{x},t)$ for t in a larger range.

TABLE 1. The L^2-norm errors for time $t = 0.5, 1, 2, \cdots, 6$ for a two-dimensional example in §4.1.

$t\backslash h$	2/16	2/32	2/64	2/128	2/256	2/512	$\|u-u_h\|_0$
0.5	1.78E-2	4.27E-3	8.91E-4	1.81E-4	2.71E-4	3.13E-4	1.13E-1 $h^{1.24}$
1	1.73E-2	4.36E-3	1.10E-3	2.80E-4	7.36E-5	2.14E-5	9.43E-1 $h^{1.94}$
2	1.57E-2	3.94E-3	9.97E-4	2.51E-4	6.45E-5	1.73E-5	9.25E-1 $h^{1.97}$
3	1.42E-2	3.57E-3	9.02E-4	2.27E-4	5.84E-5	1.57E-5	8.34E-1 $h^{1.97}$
4	1.28E-2	3.23E-3	8.17E-4	2.06E-4	5.32E-5	1.45E-5	7.43E-1 $h^{1.96}$
5	1.16E-2	2.92E-3	7.40E-4	1.88E-4	4.96E-5	1.46E-5	6.25E-1 $h^{1.94}$
6	1.05E-2	2.65E-3	6.77E-4	1.77E-4	5.16E-5	2.02E-5	4.20E-1 $h^{1.83}$

TABLE 2. The H^1-seminorm errors for time $t = 0.5, 1, 2, \cdots, 6$ for a two-dimensional example in §4.1.

$t\backslash h$	2/16	2/32	2/64	2/128	2/256	2/512	$\|u-u_h\|_1$
0.5	3.79E-1	1.90E-1	9.56E-2	4.80E-2	2.42E-2	1.23E-2	2.96 $h^{0.99}$
1	3.61E-1	1.81E-1	9.10E-2	4.57E-2	2.30E-2	1.17E-2	2.82 $h^{0.99}$
2	3.26E-1	1.64E-1	8.23E-2	4.13E-2	2.08E-2	1.06E-2	2.56 $h^{0.99}$
3	2.96E-1	1.48E-1	7.45E-2	3.74E-2	1.88E-2	9.56E-3	2.31 $h^{0.99}$
4	2.67E-1	1.34E-1	6.74E-2	3.39E-2	1.70E-2	8.65E-3	2.09 $h^{0.99}$
5	2.42E-1	1.21E-1	6.10E-2	3.06E-2	1.54E-2	7.83E-3	1.89 $h^{0.99}$
6	2.19E-1	1.10E-1	5.52E-2	2.78E-2	1.40E-2	7.08E-3	1.71 $h^{0.99}$

4.2. 1D numerical examples. Next, we consider a one-dimensional IBVP:

$$\begin{aligned} u_t - (au_x)_x &= f, \ (x,t) \in \Omega \times (0,T], \\ u(0,t) = g_0(t), \quad u(1,t) &= g_1(t), \quad t \in (0,T], \\ u(x,0) &= u_0(x), \quad x \in \Omega, \end{aligned}$$

with the domain $\Omega = (0,1)$ and the piecewise constant coefficient function $a(x)$ given by

$$\begin{aligned} a(x) &= \begin{cases} a^- = 1, & x \in \Omega^-, \\ a^+ = 20, & x \in \Omega^+, \end{cases} \\ \Omega^- &= (0, \pi/6), \ \Omega^+ = \Omega \setminus \overline{\Omega^-}. \end{aligned}$$

In all the numerical experiments, we choose $f(x,t), u_0(x)$, and $g_0(t), \ g_1(t)$ such that the exact solution of the IBVP is given by

$$\begin{aligned} u(x,t) &= \begin{cases} e^{x-0.1t}, & (x,t) \in \Omega^- \times (0,T], \\ \left(\left((x-\pi/6)^{p+1} + c_1\right)e^x + c_2\right) e^{-0.1t}, & (x,t) \in \Omega^+ \times (0,T], \end{cases} \\ c_1 &= \frac{a^-}{a^+}, \ c_2 = (1-c_1)e^{\pi/6}, \end{aligned}$$

where p is the degree of the polynomial used in the IFE spaces.

We first use $N_z = 50$ as the number of control points on the contour Γ with the same parameters as in the previous example in §4.1 for the inversion of the Laplace transform in all the numerical experiments and vary the degree of IFEs from $p = 1$ to 5. Each of the IFE spaces is formed on a uniform mesh Ω_h of Ω with $h = 1/4, 1/8, 1/16$, and $1/32$. The L^2-norm and H^1-seminorm errors and their reduction rates are shown in Tables 3 and 4.

From these data tables, we note that the convergence rate in the H^1-seminorm is optimal while that in the L^2 norm is also optimal except $p = 5$. This indicates

TABLE 3. L^2-norm errors at $t = 2$ with higher-order IFEs with $N_z = 50$ for a one-dimensional example in §4.2.

$p\backslash h$	1/4	1/8	1/16	1/32	$\|u - u_h\|_0$
1	3.10E-2	6.24E-3	1.38E-3	3.37E-4	6.01E-1 $h^{2.17}$
2	1.33E-3	1.57E-4	1.97E-5	2.22E-6	9.39E-2 $h^{3.07}$
3	8.70E-5	5.71E-6	3.17E-7	1.90E-8	2.53E-2 $h^{4.07}$
4	6.47E-6	1.90E-7	5.85E-9	2.31E-10	5.68E-3 $h^{4.93}$
5	4.57E-7	6.75E-9	1.87E-10	1.55E-10	4.75E-5 $h^{3.98}$

TABLE 4. H^1-seminorm errors at $t = 2$ with high-order IFEs with $N_z = 50$ for a one-dimensional example in §4.2.

$p\backslash h$	1/4	1/8	1/16	1/32	$\|u - u_h\|_1$
1	5.09E-1	1.76E-1	7.62E-2	3.73E-2	2.63 $h^{1.25}$
2	4.39E-2	1.07E-2	2.48E-3	5.51E-4	8.33E-1 $h^{2.11}$
3	5.02E-3	5.90E-4	5.97E-5	7.19E-6	4.09E-1 $h^{3.17}$
4	5.06E-4	2.45E-5	1.49E-6	8.67E-8	1.52E-1 $h^{4.16}$
5	4.00E-5	1.12E-6	3.27E-8	9.98E-10	4.60E-2 $h^{5.10}$

that 50 control points used in the approximation of the contour integration for the Laplace inversion are not sufficient. We numerically find that increasing the control points to about 230 enables this scheme to perform optimally for the 5th degree IFEs; see data in Tables 5 and 6.

TABLE 5. L^2-norm errors at $t = 2$ with higher-order interface elements with $N_z = 230$ for a one-dimensional example in §4.2.

$p\backslash h$	1/4	1/8	1/16	1/32	$\|u - u_h\|_0$
5	4.57E-7	6.75E-9	1.03E-10	1.72E-12	1.84E-3 $h^{6.00}$

TABLE 6. H^1-seminorm errors at $t = 2$ with higher-order interface elements with $N_z = 230$ for a one-dimensional example in §4.2.

$p\backslash h$	1/4	1/8	1/16	1/32	$\|u - u_h\|_1$
5	4.00E-5	1.12E-6	3.27E-8	9.93E-10	4.62E-2 $h^{5.10}$

In our numerical experiments, we notice again that once the complex-valued elliptic IFE solutions are prepared for the set of z_j, $j = 0, 1, \cdots, N_z - 1$ chosen on the control contour, they can be used to generate approximations to $u(x, t)$ for a long range of t. For example, when the quadratic IFEM is used with $N_z = 80$ control points, our method performs optimally for any $t \in [0.95, 15]$ as demonstrated by the error data in both the L^2-norm and the H^1-seminorms in Tables 7 and 8.

4.3. Numerical examples with large jump in coefficients. In general, a larger jump in the coefficient $a(\mathbf{x})$ across the interface implies a stronger discontinuity in the exact solution, and this usually makes the related interface problem more challenging for conventional numerical methods. On the other hand, since the jump conditions across the interface have been incorporated into IFE basis functions, the

TABLE 7. L^2-norm errors at various times with 2nd-order interface elements with $N_z = 80$ for a one-dimensional example in §4.2.

$t\backslash h$	1/10	1/18	1/26	1/34	$\|u - u_h\|_0$
0.95	1.48E-3	1.74E-4	2.19E-5	2.58E-6	1.01E-1 $h^{3.05}$
5	9.89E-4	1.61E-4	1.46E-5	1.65E-6	6.96E-2 $h^{3.07}$
15	3.64E-4	4.27E-5	5.37E-6	6.61E-7	2.39E-2 $h^{3.03}$

TABLE 8. H^1-seminorm errors at various time with 2nd-order interface elements with $N_z = 80$ for a one-dimensional example in §4.2.

$t\backslash h$	1/10	1/18	1/26	1/34	$\|u - u_h\|_1$
0.95	4.87E-2	1.19E-2	2.75E-3	6.12E-4	9.26E-1 $h^{2.11}$
5	3.25E-2	7.96E-3	1.84E-3	4.08E-4	6.17E-1 $h^{2.11}$
15	1.20E-2	2.93E-3	6.76E-4	1.50E-4	2.27E-1 $h^{2.11}$

jump magnitude in coefficient becomes a much less concern for IFEMs. This feature has been reported for several IFEMs developed for solving time independent interface problems, see [12, 19] for example. This feature seems to hold also for the IFEM developed in this article for solving parabolic interface problems.

To see this, we consider interface problems similar to the one in Section 4.1 except that the ratio $a^- : a^+$ or $a^+ : a^-$ in these problems is much larger. Tables 9 and 10 contain numerical results generated by the IFEM developed in the present article for the interface problem in which $a^- = 1, a^+ = 1000$, while Tables 11 and 12 contain numerical results for the interface problem in which $a^- = 1000, a^+ = 1$. These numerical results clearly suggest that our IFEM can perform optimally in the chosen time range. We note that, without presenting actual numerical data in order to reduce presentation space, similar behaviors of our IFEM are also observed for the 1D parabolic interface problems with large jump in the coefficients.

TABLE 9. The L^2-norm errors for time $t = 1, \cdots, 6$ for a two-dimensional example in §4.3 with $a^- = 1, a^+ = 1000$.

$t\backslash h$	1/16	1/32	1/64	1/128	1/256	1/512	$\|u - u_h\|_0$
1	3.91E-3	1.04E-3	2.78E-4	6.06E-5	1.41E-5	3.41E-6	2.98E-1 $h^{2.05}$
2	3.54E-3	9.40E-4	2.52E-4	5.48E-5	1.27E-5	2.99E-6	2.75E-1 $h^{2.05}$
3	3.20E-3	8.51E-4	2.28E-4	4.96E-5	1.15E-5	2.71E-6	2.49E-1 $h^{2.05}$
4	2.90E-3	7.70E-4	2.06E-4	4.49E-5	1.04E-5	2.46E-6	2.24E-1 $h^{2.05}$
5	2.62E-3	6.97E-4	1.87E-4	4.07E-5	9.48E-6	2.30E-6	1.99E-1 $h^{2.04}$
6	2.37E-3	6.31E-4	1.69E-4	3.70E-5	8.91E-6	2.71E-6	1.51E-1 $h^{1.99}$

5. Conclusions

We have applied the Laplace transformation method for the discretization in time and the immersed finite element method for that in space in solving linear parabolic problems with piecewise constant coefficients on structured Cartesian meshes. A linear immersed finite element is adopted for 2D examples which has jump ratios in the coefficient from 1:10 to 1:1000. High-order immersed finite elements up to degree five are employed for 1D examples. Numerical results indicate optimal

TABLE 10. The H^1-norm errors for time $t = 1, \cdots, 6$ for a two-dimensional example in §4.3 with $a^- = 1, a^+ = 1000$.

$t\backslash h$	1/16	1/32	1/64	1/128	1/256	1/512	$\lvert u - u_h \rvert_1$
1	7.03E-2	3.61E-2	1.82E-2	9.04E-3	4.54E-3	2.30E-3	5.57E-1 $h^{1.00}$
2	6.36E-2	3.27E-2	1.65E-2	8.18E-3	4.11E-3	2.08E-3	5.04E-1 $h^{1.00}$
3	5.75E-2	2.96E-2	1.49E-2	7.40E-3	3.72E-3	1.89E-3	4.56E-1 $h^{1.00}$
4	5.21E-2	2.68E-2	1.35E-2	6.70E-3	3.37E-3	1.71E-3	4.12E-1 $h^{1.00}$
5	4.71E-2	2.42E-2	1.22E-2	6.06E-3	3.05E-3	1.54E-3	3.73E-1 $h^{1.00}$
6	4.26E-2	2.19E-2	1.11E-2	5.48E-3	2.76E-3	1.40E-3	3.38E-1 $h^{1.00}$

TABLE 11. The L^2-norm errors for time $t = 1, \cdots, 6$ for a two-dimensional example in §4.3 with $a^- = 1000, a^+ = 1$.

$t\backslash h$	1/16	1/32	1/64	1/128	1/256	1/512	$\lVert u - u_h \rVert_0$
1	1.73E-2	4.34E-3	1.09E-3	2.74E-4	7.01E-5	1.97E-5	1.00 $h^{1.96}$
2	1.57E-2	3.93E-3	9.82E-4	2.46E-4	6.12E-5	1.55E-5	9.98 E-1 $h^{2.00}$
3	1.42E-2	3.56E-3	8.88E-4	2.23E-4	5.54E-5	1.41E-5	9.00 E-1 $h^{2.00}$
4	1.28E-2	3.22E-3	8.04E-4	2.02E-4	5.04E-5	1.31E-5	8.99 E-1 $h^{1.99}$
5	1.16E-2	2.91E-3	7.29E-4	1.84E-4	4.71E-5	1.35E-5	6.64 E-1 $h^{1.96}$
6	1.05E-2	2.64E-3	6.66E-4	1.74E-4	4.93E-5	1.94E-5	4.33 E-1 $h^{1.85}$

TABLE 12. The H^1-norm errors for time $t = 1, \cdots, 6$ for a two-dimensional example in §4.3 with $a^- = 1000, a^+ = 1$.

$t\backslash h$	1/16	1/32	1/64	1/128	1/256	1/512	$\lvert u - u_h \rvert_1$
1	3.61E-1	1.81E-1	9.06E-2	4.53E-2	2.26E-2	1.13E-2	2.89E-1 $h^{1.00}$
2	3.27E-1	1.64E-1	8.19E-2	4.10E-2	2.05E-2	1.02E-2	2.62E-1 $h^{1.00}$
3	2.96E-1	1.48E-1	7.41E-2	3.71E-2	1.85E-2	9.27E-3	2.36E-1 $h^{1.00}$
4	2.68E-1	1.34E-1	6.71E-2	3.35E-2	1.68E-2	8.39E-3	2.14E-1 $h^{1.00}$
5	2.42E-1	1.21E-1	6.07E-2	3.04E-2	1.52E-2	7.59E-3	1.94E-1 $h^{1.00}$
6	2.19E-1	1.10E-1	5.49E-2	2.75E-2	1.37E-2	6.87E-3	1.75E-1 $h^{1.00}$

convergence can be obtained by solving a reasonably small number of complex-valued elliptic problems, which are obtained by the Laplace transformation of the parabolic problems in time variable.

References

[1] S. Adjerid and T. Lin. Higher-order immersed discontinuous Galerkin methods. *International Journal of Information and Systems Sciences*, 3(4):555–568, 2007.

[2] S. Adjerid and T. Lin. p-th degree immersed finite element for boundary value problems with discontinuous coefficients. *J. Appl. Numer. Math.*, (submitted).

[3] T. J. I'a. Bromwich. Normal coordinates in dynamical systems. *Proc. Lond. Math. Soc.*, 15(Ser. 2):401–448, 1916.

[4] B. Camp, T. Lin, Y. Lin, and W.-W. Sun. Quadratic immersed finite element spaces and their approximation capabilities. *Adv. Comput. Math.*, 24:81–112, 2006.

[5] G. Deutch. Theorie und Anwendung der Laplace-Transformation, Berlin 1937 (Translated and abridged by W. A. Mersman); New York: Dover Publications 1943.

[6] C. C. Douglas. Madpack: A family of abstract multigrid or multilevel solvers. *Comput. Appl. Math.*, 14:3–20, 1995.

[7] C. C. Douglas, I. Kim, H. Lee, and D. Sheen. Higher-order schemes for the Laplace transformation method for parabolic problems. *Computing and Visualization in Science*, 14:39–47, 2011.

[8] R. E. Ewing, Z. Li, T. Lin, and Y. Lin. The immersed finite volume element method for the elliptic interface problems. *Mathematics and Computers in Simulation*, 50:63–76, 1999.

[9] R. W. Freund and N. M. Nachtigal. QMR: a quasi-minimal residual method for non-Hermitian linear systems. *Numer. Math.*, 60(3):315–339, 1991.
[10] I. P. Gavrilyuk, , W. Hackbusch, and B. N. Khoromskij. $\mathcal{H}$-matrix approximation for the operator exponential with applications. *Numer. Math.*, 92:83–111, 2002.
[11] Y. Gong, B. Li, and Z. Li. Immersed-interface finite-element methods for elliptic interface problems with non-homogeneous jump conditions. *SIAM J. Numer. Anal.*, 46:472–495, 2008.
[12] X.-M. He, T. Lin, and Y. Lin. Approximation capability of a bilinear immersed finite element space. *Numer. Methods Partial Differential Equations*, 24(5):1265–1300, 2008.
[13] X.-M. He, T. Lin, and Y. Lin. A bilinear immersed finite volume element method for the diffusion equation with discontinuous coefficients. *Commun. Comput. Phys.*, 6(1):185–202, 2009.
[14] R. Kafafy, T. Lin, Y. Lin, and J. Wang. 3-d immersed finite element methods for electric field simulation in composite materials. *Int. J. Numer. Meth. Engrg.*, 64:904–972, 2005.
[15] R. Kafafy, J. Wang, and T. Lin. A hybrid-grid immersed-finite-element particle-in-cell simulation model of ion optics plasma dynamics. *Dynamics of Continuous, Discrete and Impulse Systems*, 12:1–16, 2005.
[16] J. Lee and D. Sheen. An accurate numerical inversion of Laplace transforms based on the location of their poles. *Comput. & Math. Applic.*, 48(10–11):1415–1423, 2004
[17] J. Lee and D. Sheen. A parallel method for backward parabolic problems based on the Laplace transformation. *SIAM J. Numer. Anal.*, 44:1466–1486, 2006.
[18] Z. Li. The immersed interface method using a finite element formulation. *Appl. Numer. Math.*, 27:253–267, 1998.
[19] Z. Li, T. Lin, Y. Lin, and R. Rogers. An immersed finite element space and its approximation capability. *Numer. Methods Partial Differential Equations*, 20(3):338–367, 2004.
[20] Z. Li, T. Lin, and X. Wu. New Cartesian grid methods for interface problems using finite element formulation. *Numer. Math.*, 96(1):61–98, 2003.
[21] T. Lin, Y. Lin, R. C. Rogers, and L. M. Ryan. A rectangular immersed finite element method for interface problems. In P. Minev and Y. Lin, editors, *Advances in Computation: Theory and Practice, Vol. 7*, pages 107–114. Nova Science Publishers, Inc., 2001.
[22] T. Lin, Y. Lin, and W.-W. Sun. Error estimation of quadratic immersed finite element methods. *Discrete and Continuous Dynamical Systems-Series B*, 7(4):807–823, 2007.
[23] T. Lin and J. Wang. An immersed finite element electric field solver for ion optics modeling. In *Proceedings of AIAA Joint Propulsion Conference, Indianapolis, IN, July, 2002*. AIAA, 2002-4263.
[24] T. Lin and J. Wang. The immersed finite element method for plasma particle simulation. In *Proceedings of AIAA Aerospace Sciences Meeting, Reno, NV, Jan., 2003*. AIAA, 2003-0842.
[25] M. López-Fernández and C. Palencia. On the numerical inversion of the Laplace transform of certain holomorphic mappings. *Appl. Numer. Math.*, 51:289–303, 2004.
[26] D. Sheen, I. H. Sloan, and V. Thomée. A parallel method for time-discretization of parabolic problems based on contour integral representation and quadrature. *Math. Comp.*, 69(229):177–195, 2000.
[27] D. Sheen, I. H. Sloan, and V. Thomée. A parallel method for time-discretization of parabolic equations based on Laplace transformation and quadrature. *IMA J. Numer. Anal.*, 23(2):269–299, 2003.
[28] S. A. Suater and R. Warnke. Composite finite elements for elliptic boundary value problems with discontinuous coefficients. *Computing*, 77:29–55, 2006.
[29] V. Thomée. A high order parallel method for time discretization of parabolic type equations based on Laplace transformation and quadrature. *Int. J. Numer. Anal. Model.*, 2:121–139, 2005.
[30] J. Wang, X.-M. He, and Y. Cao. Modeling spacecraft charging and charged dust particle interactions on lunar surface. *Proceedings of the 10th Spacecraft Charging Technology Conference, Biarritz, France*, 2007.
[31] J. A. C. Weideman. Algorithms for parameter selection in the Weeks method for inverting Laplace transforms. *SIAM J. Sci. Comput.*, 21(1):111–128, 1999.

Department of Mathematics, Virginia Polytechnic Institute & State University, Blacksburg, VA 24061-0123, USA
E-mail: tlin@vt.edu
URL: http://www.math.vt.edu/people/tlin/

Department of Mathematics, and Interdisciplinary Program in Computational Science & Technology, Seoul National University, Seoul 151–747, Korea
E-mail: sheen@snu.ac.kr
URL: http://www.nasc.snu.ac.kr/sheen/